Landsc Ecol
https://doi.org/10.1007/s10980-023-01648-4

RESEARCH ARTICLE

Urban–rural interface dominates the effects of urbanization on watershed energy and water balances in Southern China

Kailun Jin · Mengsheng Qin · Run Tang · Xiaolin Huang · Lu Hao · Ge Sun

Received: 14 September 2022 / Accepted: 26 March 2023

Abstract

Context Quantifying the interactions between land disturbances and energy and water balances, particularly evapotranspiration (ET), is helpful for understanding the land-atmospheric interactions and assessing the effects of urbanization on local climate and hydrological processes at a landscape scale.

Objectives To investigate the mechanisms of ecohydrological response to urbanization from the perspectives of ET or energy balances in a distributed fashion at the watershed scale. To identify spatial 'hot spots', in which ET, and thus watershed hydrology, are most pronounced in response to land use change so that limited watershed landscape management resources can be applied efficiently.

Methods This process-based research quantified spatial patterns of ET and other energy fluxes in a rapidly urbanizing rice paddy-dominated watershed, Qinhuai River Basin (QRB), using a spatially explicit land surface energy balance model (SEBAL).

Results The QRB experienced a rapid land use change in urban–rural interface (URI) area, resulting in a significant reduction in actual ET ($-$ 9.4 mm yr^{-1}) but a significant increase in sensible heat (3.71 W m^{-2} yr^{-1}) and soil heat fluxes (0.85 W m^{-2} yr^{-1}) during the growing season from 2001 to 2019. The change in energy partitioning at the watershed scale was dominated by URI area identified as the 'hot spots' of ecohydrological change within a heterogeneous basin.

Conclusions Knowledge gained from this study improves parameterizing distributed watershed ecohydrological models (e.g., ET processes) to guide urban planning. Effective watershed landscape management and planning that aims at mitigating the negative impacts of urbanization should focus on URI by preserving vegetation and local wetlands (e.g., rice paddies).

Keywords Actual Evapotranspiration (ET) · Energy Balances · Land Use Change · SEBAL · Urban–Rural Interface (URI) · Qinhuai River Basin

Supplementary Information The online version contains supplementary material available at https://doi.org/10.1007/s10980-023-01648-4.

K. Jin · M. Qin · R. Tang · X. Huang · L. Hao (✉)
Collaborative Innovation Center On Forecast and Evaluation of Meteorological Disasters (CIC-FEMD)/Key Laboratory of Ecosystem Carbon Source and Sink, China Meterological Administration (ECSS-CMA), Nanjing University of Information Science and Technology, Nanjing 210044, China
e-mail: haolu@nuist.edu.cn

M. Qin
Yangzhou Meteorology Bureau, Yangzhou 225009, Jiangsu Province, China

G. Sun
Eastern Forest Environmental Threat Assessment Center, Southern Research Station, USDA Forest Service, Research Triangle Park, Durham, NC 27709, USA

Published online: 04 April 2023

Introduction

Our previous studies have documented that rapid urbanization in humid regions of southern China and the United States has caused a series of negative climatic and hydrological consequences (Hao et al. 2015; Li et al. 2020a, b). These impacts include 'Urban Heat Island (UHI) (Zhou et al. 2016a; Hao et al. 2018), 'Urban Dry/Wet Island (UDI/UWI)' (Hao et al. 2018; Huang et al. 2022), elevated storm runoff and flood risks (Hao et al. 2015; Zheng et al. 2020; Fang et al. 2020), the loss of ecosystem productivity, and water quality (Li et al. 2020a, b; Sun and Lockaby 2012). The observed and simulated meteorological, hydrological, and ecological changes in urbanized areas have been linked to the changes in land surface processes, actual evapotranspiration (ET) in particular (Sun et al. 2011a; Hao et al. 2015, 2018; Li et al. 2020a, b; Wu and Hobbs 2002; Wu 2013). These 'Black Box' watershed studies suggest that the feedbacks of ecohydrological cycle, including ET, on urbanization-associated land cover change are particularly evident in humid regions where forests or natural or constructed wetlands dominate (Hao et al. 2015; Sun and Lockaby 2012). However, few studies have examined the mechanisms of ecohydrological response from the perspectives of ET or energy balances in a distributed fashion at the watershed scale (Zheng et al. 2020; Fang et al. 2020; Gao et al. 2017). It is important to identify spatial 'hot spots', in which ET, and thus watershed hydrology, is most pronounced in response to land use change so that limited watershed management resources can be applied efficiently.

Process-based studies on water and energy balances are available to explain observed environmental impacts, such as UHI, UDI/UWI, and ecohydrological changes due to watershed disturbances (e.g., urbanization, forest removal, and climate change) (DeWalle 2000; Ebel and Mirus 2014; Jackson et al. 2009; Vose et al. 2011; Wang et al. 2012a; Yang et al. 2017, 2020). A study in China found that the land use and land cover changes induced by rapid urbanization has affected ET and hydrological cycle from 2000 to 2013 (Li et al. 2017; Xu et al. 2015). Zheng et al. (2020) found that converting rice paddies into urban uses in the Yangtze River Delta (YRD) region in southern China had greater impacts than climate change resulting in a decrease in ET. Urbanization altered the surface energy fluxes, resulting in an increase in sensible heat flux, and a decrease in net surface shortwave and long wave radiation over eastern China (Chen et al. 2015). Due to the urbanization of the Pearl River Delta in southern China, the latent heat flux showed a negative trend from 1988 to 2010 (Tse et al. 2018). In addition, Zhou et al. (2016a) concluded that the urbanization would cause a decrease in surface energy input in southeastern China.

However, previous 'Black Box' studies at a field or watershed scale have rarely focused on the spatial differential responses of water and energy balances to urbanization, which usually occurs in critical zones such as urban–rural interface (URI) (Sun and Lockaby 2012). The URI represents a tapestry of multiple interacting networks linking urban and rural areas (Browder 2002). Forests and wetlands in URI provide important ecosystem services such as recreation, water supply, and climate regulation (Hara et al. 2005; Fang et al. 2005; Vejre et al. 2010). Land use / Cover Change (LUCC) in URI areas is usually the most dramatic change in a large basin (Wang et al. 2004), which likely causes disproportionally greater impacts on water and energy balance over time than in well-developed urban areas or underdeveloped rural areas.

To better quantify the impacts of land disturbance on water and energy balance at a large area, various modeling tools have been developed in the past two decades. These models typically combine land surface features derived from remote sensing imageries and local meteorological data. Singh et al (2008) and Bastiaanssen et al (2005) compared several such models and indicated that the Surface Energy Balance Algorithm for Land (SEBAL) model (Bastiaanssen et al. 1998a, b) performed relatively well. The SEBAL model has been successfully applied to various ecosystems in more than 30 countries with an accuracy of 85% at daily and 95% at seasonal scale for the regional ET estimates (Bastiaanssen et al. 2005; Tang et al. 2013). The SEBAL model was also applied to wetland ecosystems, for example, Nansi Lake Wetland of China (Sun et al. 2011b), alpine grassland-wetland ecosystems in the headwaters of the Yellow River (Li et al. 2013), the Upper Pangani River Basin in Eastern Africa (Kiptala et al., 2013). In China, SEBAL has been applied to the Yellow River Delta (Wang et al. 2012b), Huang-Huai-Hai Plain (Yang et al. 2015) in East China, Sanjiang

Plain, southern Xinjiang (Liu et al. 2004), the upper reaches of Shule River Basin (Chang et al. 2017), the middle reaches of Heihe River Basin (Li and Zhao 2010) and the main stream of Tarim River Basin (Li et al. 2011) in north China. However, these previous studies mostly focused on arid and semi-arid regions in northern China, were limited to a short period, and only used MODIS remote sensing products with coarse spatial resolutions.

This study focused on the 'energy limited' humid regions in southern China, which has experienced rapid urbanization in the past two decades. Unlikely many regions in China, the 'water rich' Yangtze River Delta (YRD) region represent the few regions that have not been 'greening up', but have been turning 'browning' caused by urbanization (Zhang et al. 2021, 2022; Hao et al. 2018). The densely populated YRD is facing frequent floods and droughts (Guan et al. 2014; Wu et al. 2016), water shortage and pollution (Liu et al. 2007), UHI, and UDI due to the combined influences of climate change and land use change (Hao et al. 2015, 2018). The present study represents our continuous efforts (Hao et al. 2015, 2018; Qin et al. 2019; Zheng et al. 2020; Fang et al. 2020) to mechanistically quantify the environmental effects of climate and land use change from the energy balance perspectives. Our research watershed, the Qinhuai River Basin (QRB) in the YRD, is experiencing rapid climate warming, urbanization, industrialization, and population expansion (Gu et al. 2011). We focused on spatial distributions of water-energy coupling at the watershed level by integrating advanced techniques including eddy flux observations, remote sensing, and simulation using a widely used SEBAL model (Bastiaanssen et al. 2005).

Our guiding hypothesis was that the temporal effects of urbanization on energy balance varied in space across a large basin (QRB), and these spatial differences can be sufficiently identified by a spatially explicit land surface energy balance model (SEBAL). The specific objectives of this study were to: (i) evaluate the SEBAL model to quantify the spatial distribution of ET and surface heat fluxes during the growing season over the QRB; (ii) examine how urbanization over the past decades (2001–2019) has affected the ecohydrological characteristics and surface heat fluxes of the QRB; and (iii) identify the 'hot spots' of urbanization effects on the energy and water balances in a paddy field dominated watershed. Our goal was to provide better knowledge for urban planners and land managers to minimize the negative environmental effects of urbanization through watershed management.

Material and methods

Study area

This modeling study domain was the Qinhuai River Basin (QRB) with an area of 2,588 km^2 encompassing several emerging cities in Jiangsu Province, southern China (Fig. 1). Our previous watershed scale hydrologic research on the QRB during the past decade focused on overall streamflow response to urbanization and climate change (Hao et al. 2015; Zheng et al. 2020; Fang et al. 2020). As a typical paddy field-dominated river basin, QRB has experienced rapid urbanization in the past two decades amid the economic boom in the YRD region. The QRB climate is dominated by the East Asian summer monsoon climate with a hot and humid growing season for crops such as rice and vegetables. The multi-year (2003–2013) mean annual precipitation is about 1,134 mm and 70% of which falls from May to October (Hao et al. 2015). The mean annual air temperature is about 15.6 °C and potential ET is about 1,075 mm (Gu et al. 2011; Hao et al. 2015). In the past two decades, QRB has experienced global warming with mean air temperature increased at a rate of 0.44 °C per decade (Hao et al. 2015). During the same time, the urban area tripled with a decrease in paddy fields by one third (Hao et al. 2015; Fang et al. 2020; Zheng et al. 2020). QRB has heterogenous land uses dominated by croplands (irrigated and non-irrigated) followed by urban uses and water bodies.

This study focuses on the growing season, which is locally defined as May–October when rice paddies are subjected to irrigation. The growing season showed the most pronounced contrast in surface energy balances between rice paddies and urban uses (Hao et al. 2015). We used recent LUCC data (2013) to delineate rural, urban, and URI areas. In this study, we assumed that rural areas were likely be converted to other land cover type (for example, urban land) while the original urban areas remained to be relatively stable over the study period. We used urban development intensity (UI) to categorize the entire QRB into three

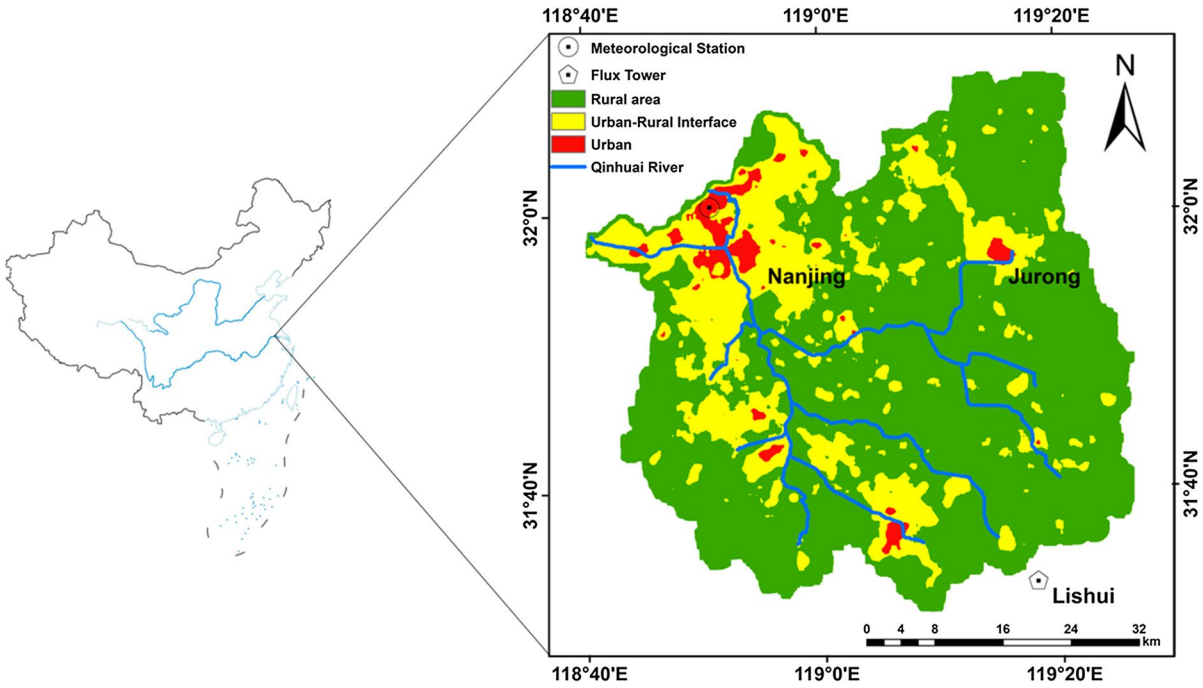

Fig. 1 Watershed locations and installations of meteorological station and eddy flux tower in Qinhuai River basin of southern China. The insert maps showed the spatial distribution of Urban, Urban–Rural Interface (URI) and Rural area based on the urban development intensity (UI) gradient in 2013

zones with different land uses. The UI was defined as the proportion of built-up land areas in each 1×1 km^2 grid cells that were scaled up from built-up land cover maps at a 30 m spatial resolution (Zhou et al. 2014; 2016a, b). Consequently, these three distinct zones for our analysis included Urban, Urban–Rural Interface (URI), and Rural with UI > 0.5, 0.15 < UI < 0.5, and UI < 0.15, respectively (Fig. 1).

The SEBAL model

The SEBAL model is a one-source model developed from simplified land surface energy balance principles (Bastiaanssen et al. 1998a):

$$LE = R_n - G - H \quad (1)$$

where LE is the latent heat flux (W m^{-2}); R_n is the net radiation flux (W m^{-2}); G is the soil heat flux (W m^{-2}); H is the sensible heat flux (W m^{-2}). Once instantaneous R_n, G, H are determined, LE and the ratio of LE/(R_n–G) or evaporative fraction can be derived. The modeling processes are illustrated in Fig. S1 and key algorithms are briefly presented below.

Net radiation flux (R_n) is calculated by the empirical formula:

$$R_n = (1 - \alpha)K_{in} + \left(L_{in} - L_{out}\right) - (1 - \varepsilon_a)L_{in} \quad (2)$$

where α α is the surface albedo which is calculated by an empirical formula with 6 bands in MOD09A1; K_{in} is the incoming short-wave radiation (W m^{-2}); L_{in} is the incoming long-wave radiation (W m^{-2}); L_{out} is the outgoing long-wave radiation (W m^{-2}); ε_a is the surface thermal emissivity computed by the normalized difference vegetation index (NDVI).

K_{in} is calculated as:

$$K_{in} = G_{sc}\cos\theta d_r \tau_{sw} \quad (3)$$

G_{sc} is the solar constant (1367 W m^{-2}), θ is the solar zenith which can be obtained from MOD09A1. d_r is the solar-terrestrial distance factor. τ_{sw} is a function about elevation of basin.

L_{in} is calculated as:

$$L_{in} = \varepsilon_0 \sigma T_a^4 \tag{4}$$

ε_0 is the atmospheric emissivity computed by the τ_{sw}. σ is the Stefan–Boltzman constant (5.67×10^8 W m^{-2} K^{-4}). T_a is a function about mean air temperature.

And, L_{out} is calculated as:

$$L_{out} = \varepsilon_a \sigma T_s^4 \tag{5}$$

T_s is land surface temperature (K) derived from remote sensing data. The Land Surface Temperature (LST) is the radiative skin temperature of the land surface, as measured in the direction of the remote sensor. LST is a mixture of vegetation and bare soil temperatures.

Soil heat flux (G) is estimated by the following empirical formula:

$$\frac{G}{R_n} = \frac{T_s - 273.15}{\alpha}\left(0.0038\alpha + 0.0074\alpha^2\right)\left(1 - 0.98NDVI^4\right) \tag{6}$$

For water bodies, G is simplified as $0.41R_n$ –51 (Burba et al., 1999) and $G = 0.3R_n$ for built-up areas. More details about modeling R_n and G in SEBAL can be found in numerous literature (Bastiaanssen et al. 1998a; Li and Zhao. 2010; Mkhwanazi et al. 2015). NDVI (Normalized Differential Vegetation Index) is derived from remote sensing data.

The SEBAL model requires two extreme crucial references representing the 'hot' and 'cold' pixels over a study area to model sensible heat flux (H) (Fig. S1). Based on NDVI, LST and land cover data, the cold pixel was selected in areas with well-watered healthy crops or shallow water bodies and the hot pixel was selected in areas with bare field or an urban area (Bastiaanssen et al. 2005; Lee et al. 2016). These two contrasting pixels were applied to compute the temperature difference (dT) between the two reference heights (Z_1 and Z_2), usually 0.1 m and 2 m. The SEBAL model assumes that dT is a linear function of T_s:

$$dT = aT_s + b \tag{7}$$

where a and b are the linear relationship constants which are defined by the two 'anchor' points where a value for H can be reliably estimated. Then, dT is used to compute H:

$$H = \frac{\rho_a C_p dT}{r_{ah}} \tag{8}$$

where ρ_a is the air density (kg m^{-3}); C_p is the air specific at constant pressure (1004 J kg^{-1} K^{-1}); r_{ah} is the aerodynamic resistance to heat transport (s m^{-1}) which is calculated as:

$$r_{ah} = \frac{1}{u^* K} ln\left(\frac{Z_2}{Z_1}\right) \tag{9}$$

in which K is the von Karman's constant (0.41) and u^* is the friction velocity (m s^{-1}) calculated by:

$$u^* = \frac{KU_x}{ln(\frac{Z_x}{z_{0m}})} \tag{10}$$

where U_x is the wind speed at a 200 m height computed by the measured wind speed at the ground meteorological station; Z_{0m} is the surface roughness length (m). The details in computing U_x and Z_{0m} can be found in the previous literature (Yang et al. 2015; Bastiaanssen et al. 1998a; Li and Zhao 2010).

The SEBAL model adopted the Monin–Obukhov length (L) to examine the stability conditions of the atmosphere and then corrected the u^* and r_{ah} with the stability correction factors $\psi_{m(200)}$, $\psi_{h(Z2)}$, and $\psi_{h(Z1)}$. The three factors are calculated following Bastiaanssen et al. (1998a, b) and Yang et al. (2012). The corrected u^* and r_{ah} are used to recalculate H, in order to make r_{ah} stable (Bastiaanssen et al. 1998a, b; Yang et al. 2012).

The LE or ET estimated by a remote-sensing-based model such as SEBAL represents an instantaneous energy flux. To estimate daily (denoted as ET_d) or longer period ET, the instantaneous LE or ET must be extrapolated temporally for a period of 24 h or more. In this study, we followed the evaporative fraction method (Jackson et al. 1981, 1983) to estimate ET_d assuming that the evaporative fraction (EF) (LE/(R_n–G)) remained constant throughout a day (Crago 1996). Therefore, we can calculate ET_d on the daily scale.

$$ET_d = \frac{86400 \times EF \times (R_{nd} - G_d)}{\lambda} \tag{11}$$

where, 86,400 is the number of seconds in a 24 h period, R_{nd} is daily net radiation flux (W m^{-2}) calculated by an empirical equation (Allen et al. 1998), G_d

is daily soil heat flux (W m^{-2}) and is negligible in a 24 h period (Bastiaanssen et al. 2002, 2005), and λ is the latent heat of vaporization, 2.45 J kg^{-1}. EF can be calculated as:

$$EF = \frac{LE}{R_n - G} \tag{12}$$

Similar principle was used for estimating actual ET at a certain period. Du et al. (2013) suggests that the ratio of actual ET (ET_a) to FAO Grass Reference ET ($R_{day} = ET_a/ET_o$) throughout a day is rather similar. Thus, ET_a determined at any time of the day by SEBAL can be conveniently scaled up to the daily (24 h) time scale using R_{day} and reference ET (ET_o). The reference ET (ET_o) was calculated by the FAO-56 Penman–Monteith model (Allen et al. 1998) with meteorological data alone.

In this study, we calculated the total ET_a for a certain period assuming a constant R_{day} for that period (Du et al. 2013; Yang et al. 2012). The total ET_a for a certain period (ET_{period}) was computed as following:

$$ET_{period} = \sum_{day=1}^{day=n} ET_{o\_day} R_{day\_s} \tag{13}$$

ET_{period} is the total ET in a certain period, n is the number of days in the period, generally 8–16 days in this study. ET_{o_day} is the daily ET_o in the period. R_{day_s} is the daily R_{day} in this period and R_{day_s} is estimated by linear interpolation using the start and end R_{day} values.

Remote sensing data

In this study, we used Terra MODIS remote sensing data to drive the SEBAL model. Data sets included 8-day albedo (MOD09A1) at a spatial resolution of 500 m, 8-day NDVI (MOD09Q1) with a resolution of 250-m and 8-day land surface temperature (MOD11A2) with a 1000 m resolution. Three MODIS products were downloaded from Land Processes Distributed Active Archive Center (https://lpdaac.usgs.gov/data_access/data_pool) and resampled at a 250-m spatial resolution using the MODIS Reprojection Tool. The land use conversion maps with a 30-m spatial resolution were derived from the Landsat 7 ETM + image (2000–9-16) and Landsat 8 OLI (Operational Land Imager) image (2013–8-11) (Fig. 2b, c) provided by USGS Earth Explorer (https://earthexplorer.usgs.gov/). The daily meteorological data for the study area were provided by the China Meteorological Data Sharing Service System (http://data.cma.cn/en). The daily meteorological data during 2001 to 2019 from 137 standard weather stations (http://data.cma.cn/) in or around the QRB were interpolated to 250 m for running SEBAL model. Necessary variables included wind speed (m/s), relative humidity (%), sunshine duration (h), maximum and minimum temperature (T_{max} and T_{min}, °C), and air pressure (hPa).

Eddy covariance measurements of energy and water fluxes for model validation

An eddy covariance measurement system was installed to monitor the surface heat and water fluxes at a rice paddy site managed by the Lishui Plant Research Station of Jiangsu Academy of Agricultural Science (31°36′N, 119°12′E). The system was equipped with CNR4 (Kipp and Zoneb, Netherlands), CAST 3 (Campbell Scientific, USA), LI-7500 (LI-COR, USA). Measured R_n, LE (i.e., ET), and H during 2016 – 2018 were used to evaluate the performance of the SEBAL model. The SEBAL results were spatial averaged across 3 × 3 paddy field pixels in QRB compared with Lishui flux tower in growing season.

The 30-min eddy covariance energy flux data were processed with the EddyPro software (Fratini and Mauder 2014). The linear regression of least square and energy residual methods were used to evaluate the energy balance closure and quality of flux data for the rice growing season (Verma et al. 1986). The slope of the fitting line of the 2018 observation data is 0.52, the intercept is 27 W m^{-2}, and the determination coefficient R^2 is 0.82 (Fig. S2a). The energy residual D indicates energy balance closure. The average daily change range D is –56 ~ 219 W m^{-2}, with the average value of 38.6 W m^{-2} (Fig. S2b). The D value during night is negative with little fluctuation, while D value at day time is positive with great fluctuations. At sunrise and sunset, the D value is the smallest while the maximum value of D occurred in middle day. These energy flux and balance measurement statistics of R^2 and regression slops for energy closure were comparable to that in Liu et al. (2017) who conducted a similar study for paddy fields in the

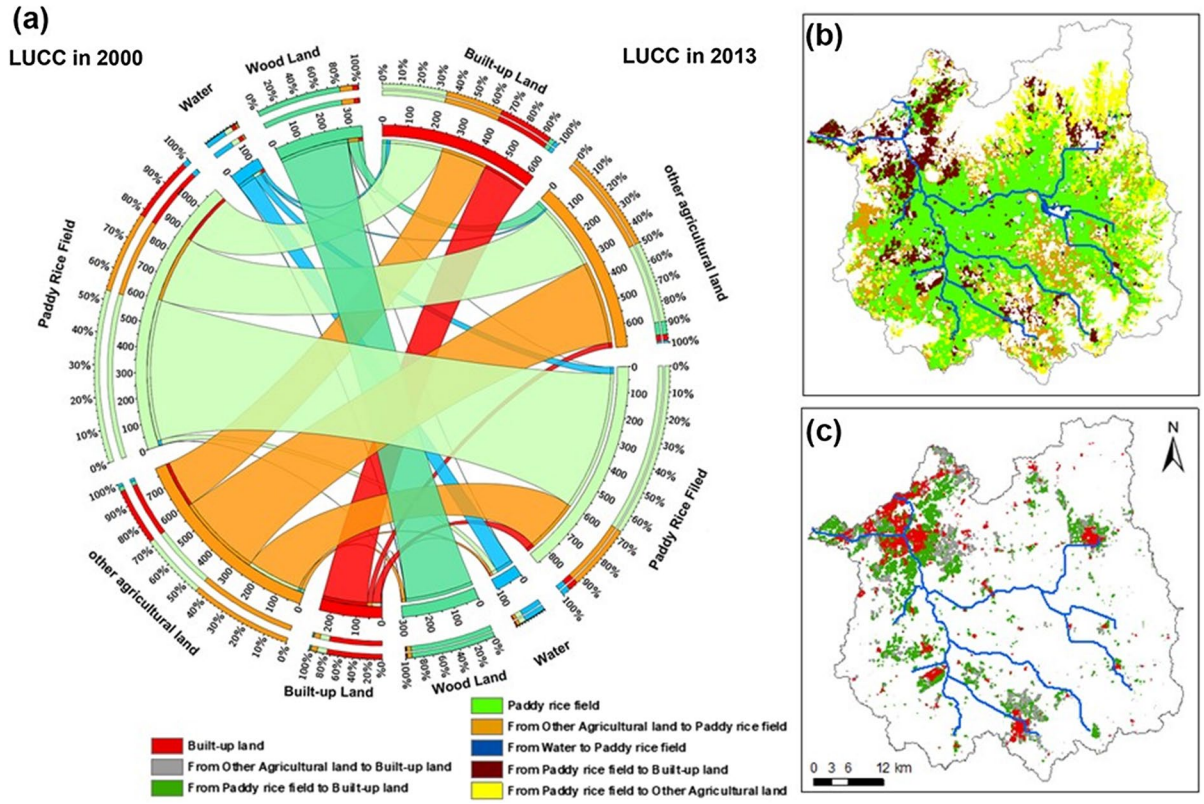

Fig. 2 **a** The Circos image (created at http://mkweb.bcgsc.ca/tableviewer/visualize/ (Krzywinski et al. 2009)) presents the area of LUCC conversion in Qinhuai River Basin. Land use conversion patterns based on **b** paddy rice fields, and **c** built-up lands from 2000 to 2013. The spatial resolution is 30 m

same region. The low R^2 at a 30-min time scale was mainly due to 1) the complex underlying surface of paddy field where unaccounted surface water and soil heat storage change can be an important component, and 2) inherent measurement errors of the eddy flux system and equipment for measuring net radiation.

Remote sensing-based estimates of ET for model validation

For validating the SEBAL model, in addition to use site-level eddy flux measurements, we also used two remote sensing ET products at the watershed level. The improved MOD16 data sets provide consistent estimates of global actual ET at an 8-day and 1-km^2 resolution (Mu et al. 2011). Actual evapotranspiration (ET) at monthly and 1-km^2 resolution data based on the Operational Simplified Surface Energy Balance (SSEBop) model (Senay et al. 2013) was also used to validate the SEBAL model and identify ET trend from 2003 to 2019. The SSEBop dataset includes ET estimates over urban areas in contrast to the raw MODIS ET products (i.e., MOD16A2) that exclude urban areas (Mazrooei et al. 2021). SSEBop ET results compared reasonably well with monthly eddy covariance ET data explaining 64% of the observed variability across diverse ecosystems in the CONUS, which suggested that this dataset is reliable for continental studies and applications (Senay et al. 2013).

Land use change across the watershed

Land uses changed dramatically within the QRB during the study period 2000–2013 (Fig. 2a). The area of Paddy Rice Field was 1092 km^2 (42.2% of the whole basin) in 2000 and decreased by 21.1% to 861 km^2 (33.2% of the whole basin) in 2013. The Paddy Rice Field had the largest relative reduction mainly due to

conversion to Built-up and Other Agricultural Land (217 km^2) (Fig. 2c, b). The Built-up land was 245 km^2 (9.5% of the whole basin) in 2000 and increased by 156% to 627 km^2 (24.2% of the whole basin) in 2013. The Built-up land was mainly converted from Paddy Rice Field (216 km^2) and the Other Agricultural Land (192 km^2) (Fig. 2a, c). The conversion from Rice Field to the Other Agricultural Land moderated the reduction of the Other Agricultural Land (Fig. 2). Additionally, conversions from vegetated covers to the Built-up land mostly occurred within the URI area (Fig. 1).

Results

Model validation

We used the measured ET_a in three years, 2017, 2018 and 2019, to assess SEBAL performance at a daily scale. There were significant correlations ($p < 0.05$) between the simulated and measured ET_a ($R^2 = 0.84$) (Fig. 3). The mean relative error of the simulated ET_a was 17.7% (Fig. 3). Overall, across the QRB, modeled ET_a by the SEBAL model was 16.2% higher than that MOD16 ET during the rice-growing season at the basin scale from 2003–2019. Annually (growing season only), the average absolute mean difference was 72.9 mm (Fig. S3). This difference was likely caused by the fact that MOD16 ET products do not include built-up areas (Fig. S4a, b) such as urban centers, e.g., the cities of Nanjing, Jiangning, Lishui and Jurong (Fig. 1). We also compared the SEBAL ET_a with SSEBop ET_a products. The result presents better between these two actual ET products. The average absolute mean difference was 31.1 mm (Fig. S3) and SEBAL ET_a was higher than SSEBop ET_a (about 6.8%).

Surface heat fluxes by land cover type

In the growing season, there were large differences among the surface energy fluxes among land use types (Fig. 4). The spatially averaged R_n was about 609.1 W m^{-2} over QRB with the highest value found in Woodlands (619 W m^{-2}) (Fig. 4a). The lowest R_n was found in the Built-up Land and Other Agricultural Land with the values of 599.9 and 607.5 W m^{-2}, respectively (Fig. 4a). The spatial averaged H was

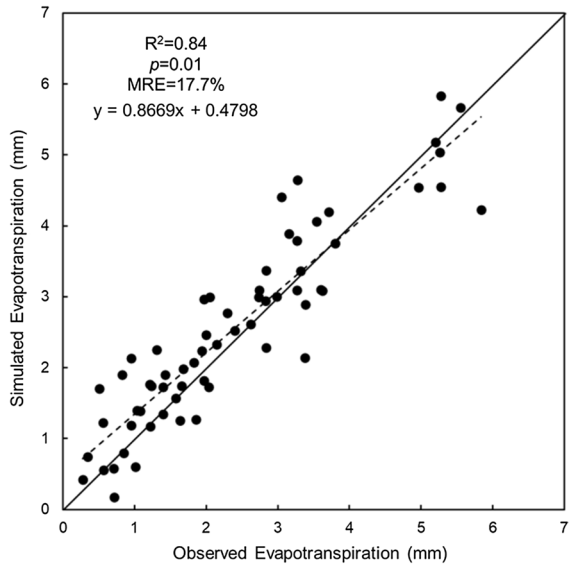

Fig. 3 Comparisons of daily actual evapotranspiration (ET_a) between SEBAL estimated and eddy covariance flux measured in Lishui Station (location see Fig. 1) in the growing seasons (May–October) from 2017 to 2019

234.8 W m^{-2} in this basin and the highest H was found over the Built-up Land with the mean value of 294.9 W m^{-2} (Fig. 4b). It was much higher than that over the other land use types with the values between 168.8 W m^{-2} (Woodland) and 217.1 W m^{-2} (Other Agricultural Land) (Fig. 4b). In contrast, LE was the lowest (225.7 W m^{-2}) in the Built-up Land (Fig. 4c). For the other land use types, LE ranged from 300 (Paddy field Land) to 385.9 W m^{-2} (Woodland) (Fig. 4c). The spatially averaged soil heat flux G was about 75.3 W m^{-2} which was the smallest among all the surface heat fluxes. The order of the soil heat fluxes G in different land use types was: Built-up Land > Paddy Rice Field > Other Agricultural Land > Woodland, with the values of 82.1, 75.4, 73.1 and 62.9 W m^{-2}, respectively (Fig. 4d).

Changes of energy balances

Spatial and temporal trends of surface heat fluxes and energy balances

The growing season R_n had a decreasing trend in URI but was stable in most of the Urban and Rural areas during 2001–2019 (Fig. 5a). The sensible heat flux (H) had an increasing trend over the URI area and

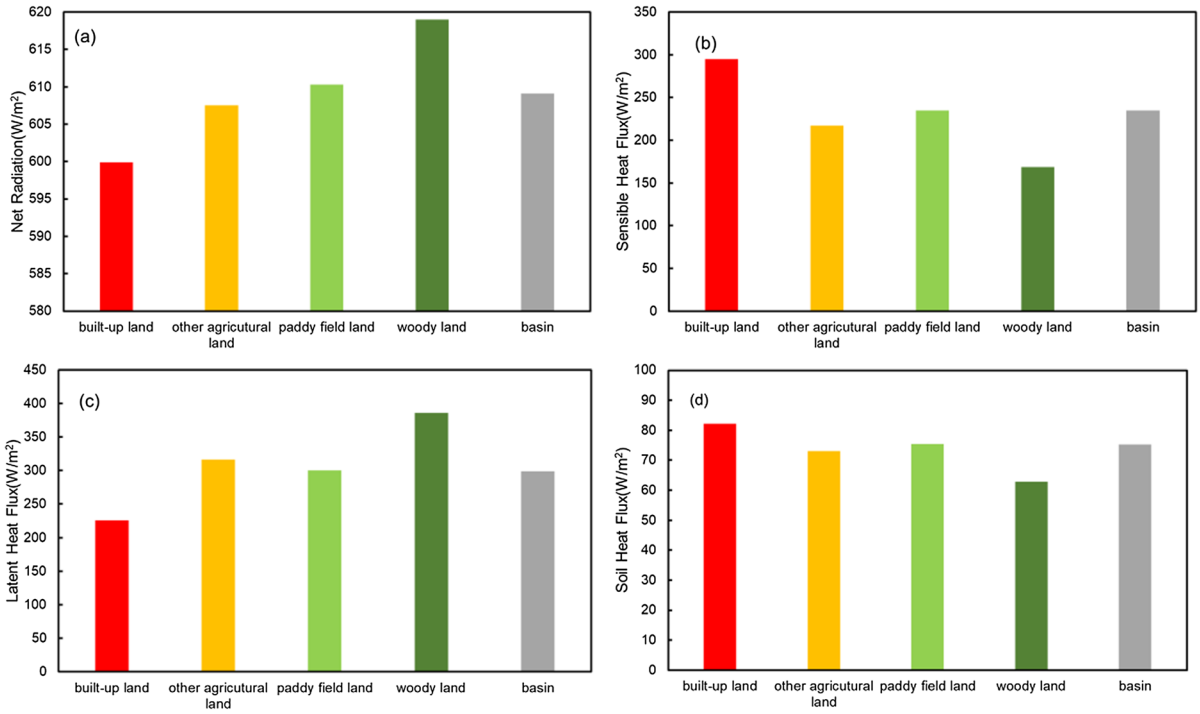

Fig. 4 Comparisons of **a** net radiation flux R_n, **b** sensible heat flux H, **c** latent heat flux LE, and **d** soil heat flux G for the growing season over different land covers (2014) in Qinhuai River basin. The reason for choosing 2014 is that in 2014, the available remote sensing data is the most reliable without cloud interference

a decreasing trend in the areas around basin's edges (Fig. 5b). In contrast, the latent heat flux (LE) exhibited an increasing trend over the areas in which the H decreased. The growing season LE decreased over the URI area (Fig. 5c). As mentioned above, the soil heat flux G increased over most areas (Fig. 5d).

The spatial mean R_n significantly decreased ($p<0.05$) in the URI area at a rate of -1.38 W m^{-2} yr^{-1}. For the Urban and Rural areas, the spatially averaged R_n decreased by lower slopes of -0.93 and -0.8 W m^{-2} yr^{-1}. All these changes led to the decreased R_n (-0.9 W m^{-2} yr^{-1}, $p<0.05$) at the basin scale (Fig. 6a). The spatial mean H displayed positive trends and negative trends over the Urban and Rural areas with a rate of 2.1 and -1 W m^{-2} yr^{-1}, respectively, while it increased by 3.71 and 0.2 W m^{-2} yr^{-1} over the URI area ($p<0.05$) and the whole basin (Fig. 6b). Similar to R_n, a decreasing trend ($p<0.05$) of spatially averaged LE was found over the URI area at a rate of -5.82 W m^{-2} yr^{-1} during 2001–2019. Less decrease over Urban area and Basin were also found to be -3.31 W m^{-2} yr^{-1} and -1.94 W m^{-2} yr^{-1} (Fig. 6c). It was noticed that the spatially averaged soil heat flux (G) in the rural area, URI area, Urban area and the whole basin all showed increasing trends ($p<0.05$), with a rate of 0.34, 0.85, 0.83 and 0.49 W m^{-2} yr^{-1}, respectively. (Fig. 6d).

The mean Bowen Ratio (BR) (H/LE) at the watershed level showed a significant positive trend over the URI area. However, BR had little change in most Rural areas (Fig. 5e). Correspondingly, the spatially averaged BR over URI and Urban area had increasing trend ($p<0.05$) with the slope of 0.11 yr^{-1} and 0.14 yr^{-1}. The spatial averaged BR over Urban area increased ($p<0.05$) with a slope of 0.04 yr^{-1}. There was slightly change in averaged BR at the basin scale (Fig. 6e).

Changes of energy flux relative to R_n

During 2001–2019, the proportion LE to R_n (LE/R_n) in the growing season ranged from 51.5% (2001–2003) to 48.7% (2017–2019) over QRB with a decrease rate of -0.21% yr^{-1}. In contrast, H/R_n at the basin

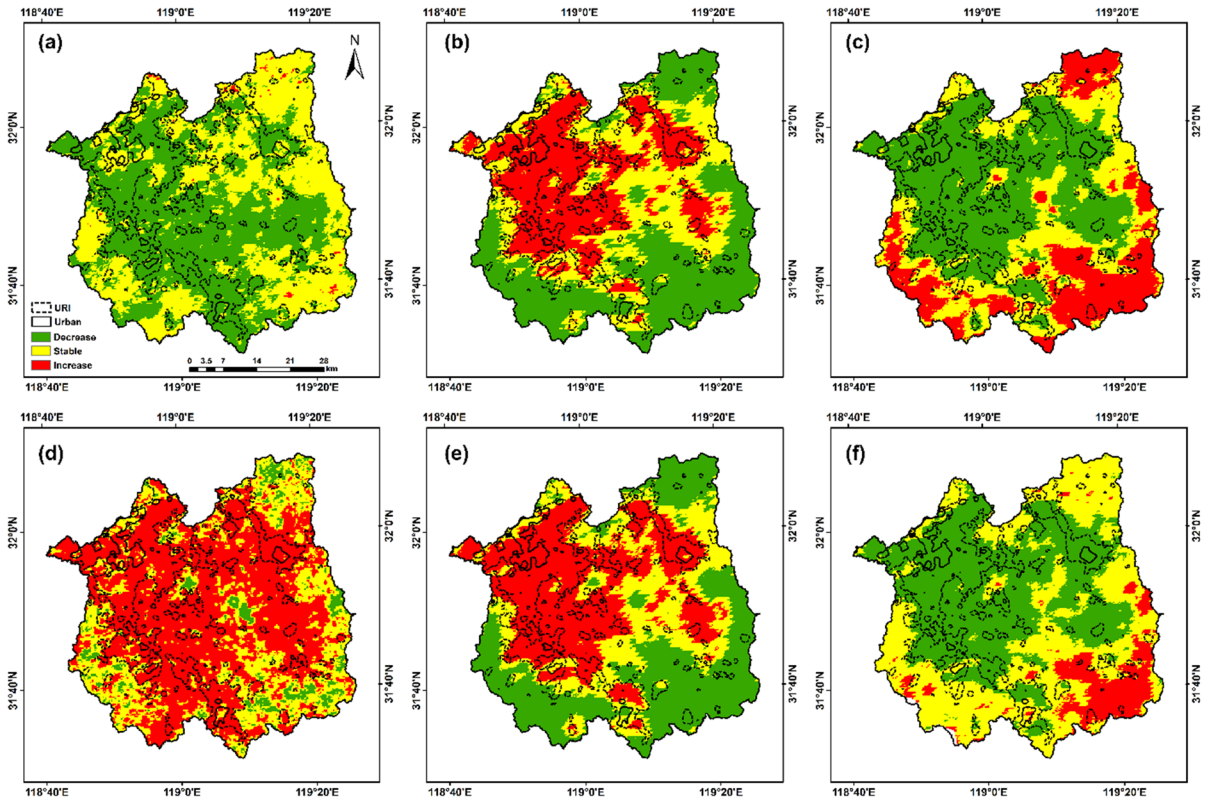

Fig. 5 The spatial distribution of modeled trends of **a** net radiation flux (R_n), **b** sensible heat flux (H), **c** latent heat flux (LE), **d** soil heat flux (G), **e** Bowen ratio (BR), and **f** actual evapotranspiration (ET_a) for the growing season in Qinhuai River basin from 2001 to 2019.The Urban and Urban–Rural Interface outlines were delineated using 2013 land cover data

level increase at a rate of 0.11% yr^{-1}. H accounted for the second largest proportion of R_n and ranged from 36.7% (2001–2003) to 37.5% (2017–2019) (Fig. 7). The soil heat flux G accounted for the smallest proportion of the R_n (11.2–14.9%) and increased by 0.1% yr^{-1} over QRB (Fig. 7). From the perspective of basin scale energy balance, the decreased LE, which was dominated by the decline of LE in the URI area, resulted in an upward trend in H and G at the basin scale, and the rising rate of H is much higher than G.

Spatial and temporal trends of ET_a in three land use zones

Because that 2002 and 2014 had the most reliable cloud-free satellite imageries than other years, we examined the change in spatial distribution of ET_a in the growing season for these two years (Fig. 8). The highest ET_a (> 600 mm) was found in the Rural area that was dominated by Woodland, Other Agricultural Land, and Paddy Rice Field with months of irrigation. The lowest ET_a was found over Urban area (< 340 mm). The ET_a rates in the URI area surrounding the Urban area were intermediate. Due to the rapid expansion of Build-up Land in our study period (Fig. 2), the area with low ET_a (< 340 mm) in 2014 was much larger than that in 2002.

The URI area showed a decreasing trend in ET_a during 2001–2019 while most of the Urban area showed an increasing trend. ET_a was stable over most Rural Zone except for the southeastern of the basin where ET_a showed an increasing trend (Fig. 5f). On average, ET_a in the URI Zone had a significantly decreasing trend ($p < 0.05$) with a rate − 9.4 mm yr^{-1} (Fig. 6f). Totally, ET_a decreased from 510 mm in 2001 to 340.8 mm in 2019. In addition, spatial averaged ET_a of Urban Zone showed a decreasing trend with the slope of − 6.2 mm yr^{-1} during the period of 2001–2019 (Fig. 6f). The Rural Zone had a slightly decreasing rate of spatially averaged ET_a

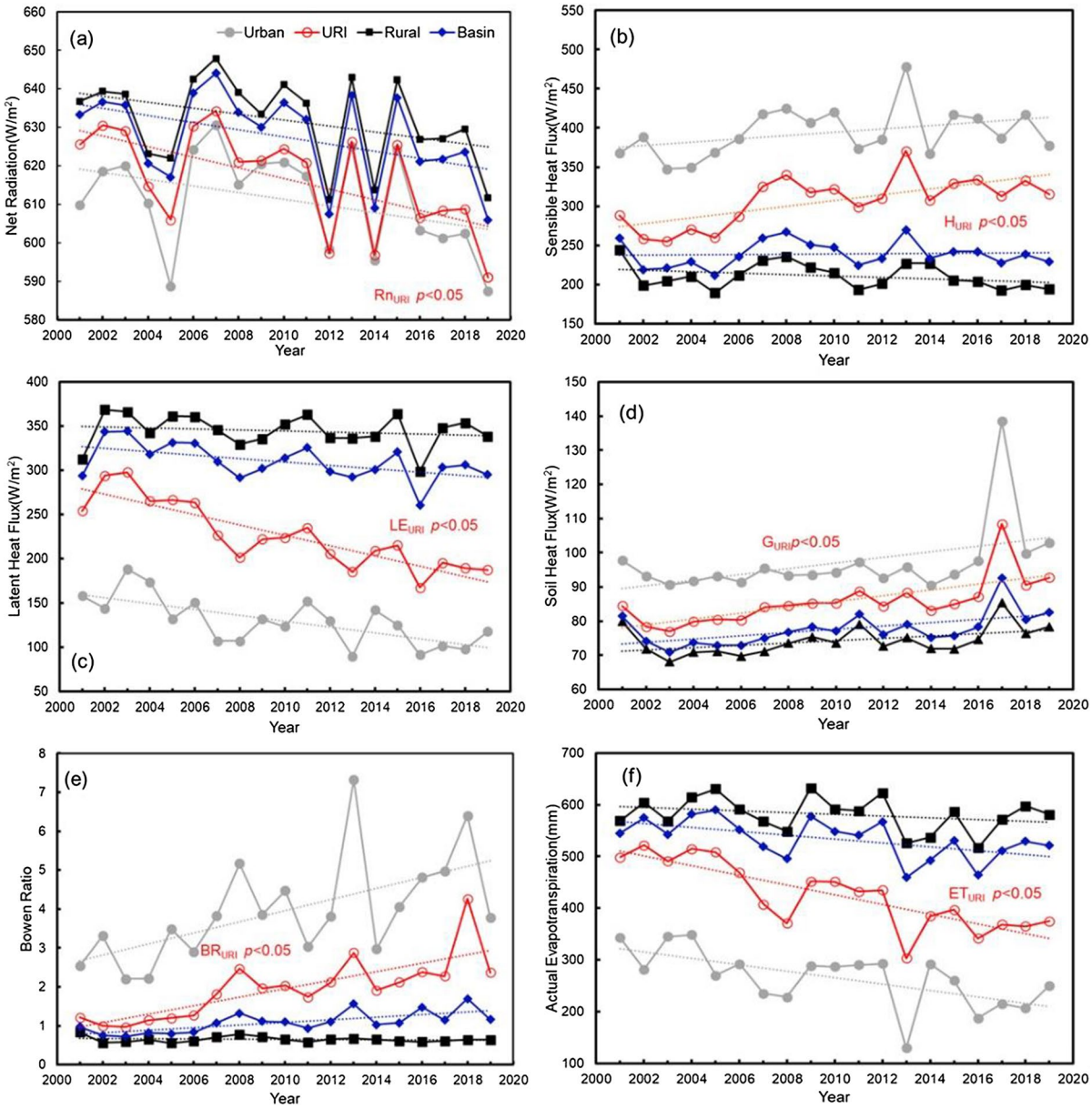

Fig. 6 Variations of the spatial averaged **a** net radiation flux (R_n), **b** sensible heat flux (H), **c** latent heat flux (LE), **d** soil heat flux (G), **e** Bowen ratio (BR), and **f** actual evapotranspiration (ET_a) for the growing season over Urban area, Urban–Rural Interface (URI) area, Rural area and the whole Qinhuai River basin from 2001 to 2019. The linear fitted trends are presented for the growing season actual evapotranspiration (ET_a)

(− 1.7 mm yr^{-1}) over the Rural area. For the entire basin as a whole, a significant ET_a decreasing trend (− 3.7 mm yr^{-1}, $p<0.05$) was mainly caused by the sharp decrease in ET_a in URI area and decreasing trend in the Urban Zone (Fig. 6f).

We also calculated the proportion of annual ET_a of three zones to the total annual ET_a in the whole basin respectively to estimate its actual impacts in an absolute term from the changes in URI at the basin scale (see Fig. S3 in Supplementary Information). We found that the proportion of ET_a in URI to the total

Fig. 7 The mean proportions of each surface heat fluxes of the net radiation flux (R_n) over the Qinhuai River basin from 2001 to 2019

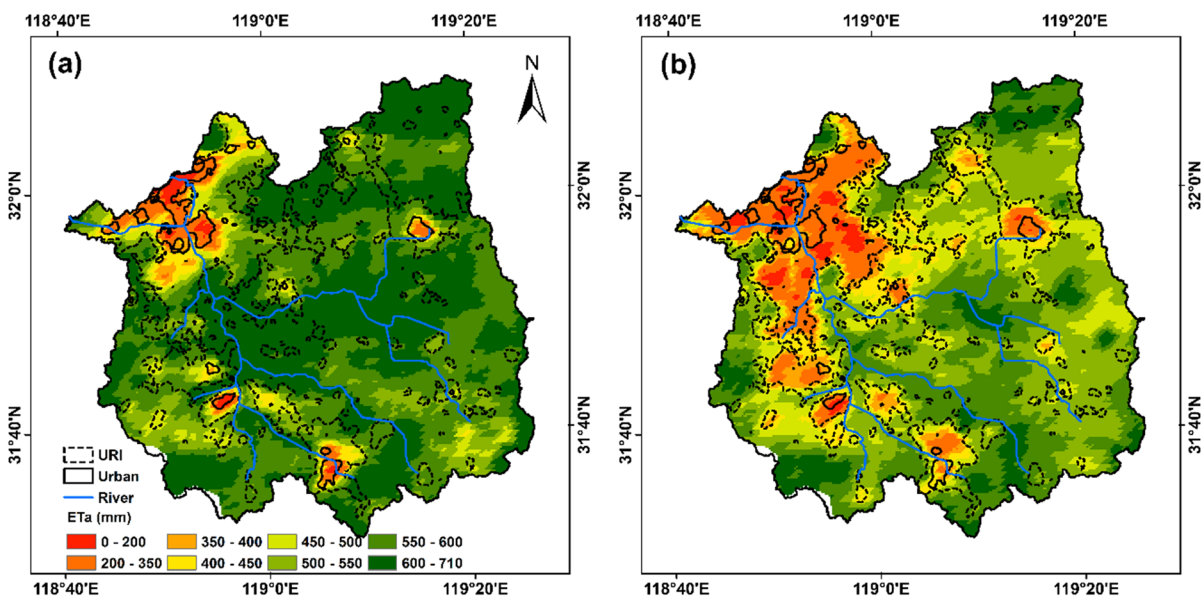

Fig. 8 The spatial distribution of SEBAL estimated actual evapotranspiration (ET_a) for the growing season in Qinhuai River basin in **a** 2002 and **b** 2014. The Urban and Urban–Rural Interface outlines were delineated using 2013 land cover data

ET_a in the whole basin was decreasing most from 2001 to 2019. This result supports our conclusion again that the change in energy partitioning at the watershed scale was dominated by URI area.

Influences of meteorological factors on ET_a under urbanization

To tease out the meteorological effects as represented by ET_o on ET_a and to examine the effects of land cover change alone, we randomly selected 200 sample points in the paddy rice fields that did not change over time and areas that converted to urban built-up from paddies during 2001–2019 (Fig. 9). The ET_o increased at a rate of 0.3 mm yr^{-1}, presumably due to climate warming (Qin et al. 2019; Hao et al. 2015). Similarly, ET_a for the selected paddy rice fields showed an upward trend while the rising rate of ET_o was 2.9 mm yr^{-1}. However, areas where paddy fields were converted to build-ups, ET_a had a decrease rate of − 4.6 mm yr^{-1}.

In general, regional annual ET is controlled by ET_o, precipitation, and land surface conditions (Sun et al. 2005; Xiang et al. 2020). A decrease in ET_a is normally caused by a decrease in precipitation and/or ET_o. Our data suggested that the decrease in ET_a

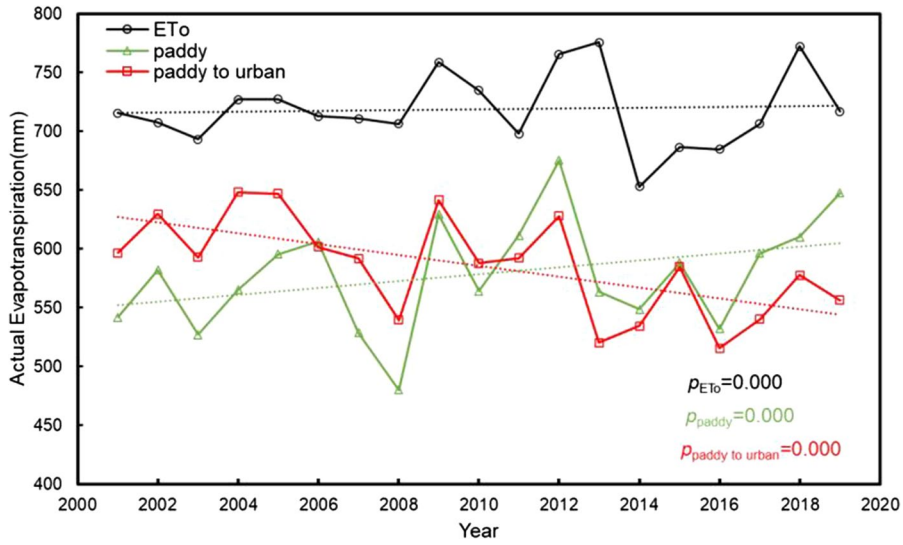

Fig. 9 Reference evapotranspiration ET_o and actual evapotranspiration ET_a in two types of rice paddy fields that experienced different land cover changes in Qinhuai River basin (2001–2019). Only the converted rice paddy field areas showed a significant decreasing trend in ET_a

in URI and Urban areas was not caused by ET_o or precipitation because the ET_o had an increased trend while overall precipitation did not change significantly (Hao et al. 2015; Zheng et al. 2020).

Discussion

Terrestrial ET variations are often a result of combined effects of climate change and land cover change (Yang et al. 2016). Using the distributed energy balance model and long-term meteorological data, we showed that ET_a changed both spatially and temporally as a result of the combined effects of urbanization and climate change and variability in a watershed dominated by a humid climate. The overall decrease in watershed-level ET_a was dominated by the decrease in ET_a in URI. Apparently, the effects of land use change overwhelmed that of climate change in the study basin as indicated by the ET_a and ET_o trend analysis (Fig. 9). Our results indicated that climate warming increased the potential ET and actual ET for areas not affected by urbanization. However, the reduction of paddy field area led to the overall reduction of ET despite the rise in potential ET at a watershed scale.

Spatially explicit mapping of energy and water fluxes allowed us to pin down the 'hot spots' of environmental change, and most importantly, the dominant causes behind the energy and water balance changes. Previous 'Black Box' studies mostly focused on climate or land use change alone and thus could not tease out the hydrological effects of LUCC from climate change (Zhan et al. 2005; Gao et al. 2017; Yang et al. 2012; Zhang et al. 2017a). Similarly, previous remote sensing-based studies often had a short period with little land-use change and thus could not detect large changes in ET trend at the watershed level (Li et al. 2010; Sun et al. 2011b; Du et al. 2013; Yang et al. 2015; Lee et al. 2016). In contrast, QRB has gone through both climate change and rapid urbanization (Gu et al. 2011) during the study period and thus offered a unique opportunity to examine the separate effect of climate change and land use change on ET and energy fluxes.

Spatial variations of trend of ET_a within a watershed

This study showed that the temporal trend of ET_a varied across space. This variable trend among Urban, Urban–Rural Interface, and Rural zones was a combined result of climate change and land use change in this heterogeneous watershed. In the Urban area and whole basin of QRB, the negative trends of ET during 2001–2019 (Fig. 6f) were consistent with the findings in eastern China such as middle part of the Yangtze River Basin where urbanization caused 'browning' and impacts on physical properties and ecohydrological processes at the land surfaces (Zhan et al. 2005; Gao et al. 2007; Yang et al. 2012; Zhang et al. 2017a).

We also noticed an increase trend with ET in southeastern part of QRB (Fig. 5). This area was

dominated by dry land, paddy field land and forest land and less impacted by urbanization. The rise of ET was likely due to the accelerated global warming and increase in atmospheric water demand (Qin et al. 2019). For humid regions in southern China, the increased temperature and wind speed are responsible for the positive trend of ET (Zhang et al. 2017b). Additionally, ET_o was also considered to be a factor which produced the major impact on controlling the variation of ET over irrigated areas (Yang et al. 2012).

In contrast, the sharp decline of ET over URI area found in this study was consistent with our previous watershed-level, empirical and modeling hydrological water balance studies in QRB (Hao et al. 2015; Fang et al. 2020; Zheng et al. 2020). Decrease trends in ET were found in rapid urbanization regions such as the North Plain areas around Beijing (Li et al. 2013), Haihe River basin of Beijing-Tianjin-Hebei Region (Gao et al. 2012), and the most areas of the populous eastern and southern China (Gao et al. 2007; Zhang et al. 2017a).

Variations of surface heat fluxes explained ET_a response to land use change and climate change

Quantifying the response of energy fluxes to urbanization helps understanding the hydrological feedbacks on the rapid expansion of built-up land areas (Yang et al. 2017; Li et al. 2017). For this study, the changes in ET_a were closely coupled with change in energy fluxes (i.e., R_n, H).

Among the three land use zones, URI showed the most decrease in R_n (Fig. 6a). This result is generally consistent with previous urbanization studies in three megacities in eastern China (Zhang et al. 2004), the Yangtze River basin in southern China (Xu et al. 2006) and the Jinghe River basin in northern China (Wang et al. 2012b). Our results support the notion that urbanization reduces R_n through altering land surface albedo and LST (Bastiaanssen et al. 1998a, b; Du et al. 2013; Zhou et al. 2016a). The significant increase in albedo and LST due to rapid urbanization (Li et al. 2011; Zhou et al. 2016a) would lead to an increase in outgoing short-wave and long-wave radiation, followed by a reduction in R_n at the basin scale. The decrease in R_n at the basin scale contributed to the decrease trend of LE. The growing season sensible heat flux H showed an upward trend over the URI and Urban areas during 2001–2019. (Fig. 6b). Besides, H showed an increasing trend at the whole basin scale in QRB (Fig. 6b). Our results are similar to those findings in central and southwestern China (Li et al. 2014; Li and Ma 2015). Wang et al. (2013) suggested that the variation of H was negatively correlated with air temperature and positively correlated with wind speed and LST. Land air temperature difference was also considered to be an important factor in variation of H (Huang et al. 2017). Therefore, we hypothesized that converting the vegetated surfaces into built-up lands within the URI area would cause an increase in LST and an increase in H in URI area. This further led to the increased H at the basin scale. Consequently, the decrease of LE in URI and Urban area is the main reason that led to the decreased LE at the basin scale in QRB (Fig. 6c). It is worth mentioning that the LE and H variation in Rural areas showed a slight trend as these areas were mostly affected by climate alone. The Rural zone might have contributed to mitigating 'urban heat islands' in URI and Urban Zone (Yan and Zhou 2023).

Soil heat flux (G) is an important component of surface energy balance and meteorological modeling (Hsieh et al. 2009). However, compared with the other three surface heat fluxes (R_n, LE, H), few studies have examined the long-term dynamics of soil heat flux under environmental change in southern China. In this study, the mean watershed-level soil heat flux in the growing season showed a significantly increasing trend in all three different land use zones with most pronounced in URI area (Fig. 6d). The increase in soil heat flux in URI was mainly caused by the increased LST (Bastiaanssen et al. 1998a, b), and the decreased NDVI, both of which were induced by rapid urbanization.

Comparison of multiple ET estimation methods

In this study, we used multiple methods to constrain the estimates of ET distribution in time and space. We compared several ET products derived with different algorithms, such as Penman–Monteith-based model (MOD16), surface energy balance-based model (SSEBop, SEBAL). We found that there were large uncertainties of global ET products used for watershed scale ET estimation.

In lieu of spatial measured ET data, we used MOD16 ET and SSEBop products to verify SEBAL

model. However, such remote sensing-based ET data may have uncertainties. For example, Jiang et al. (2017) found that MOD16 ET underestimated ET by more than 20 mm per month with bigger errors in watersheds with high ET rate in China. Feng et al. (2012) also found that MOD16 ET rates were rather low in the arid area of the Loess Plateau in China. The modeled SEBAL ET rate in this study was 16% higher than that of MOD16 ET (Fig S4). Thus, we believe that MOD16 ET products also underestimated actual ET in QRB where growing season ET was the main component of water balance in this humid area.

Thus, based on our study and the literature, we argue that the underestimation of MOD16 ET and SSEBop might be caused by the following reasons: i) the resolution (1 km^2) of meteorological reanalysis data used in MOD16 and SSEBop is too coarse for the local watershed level analysis, such as the QRB in this study; ii) the mixed pixels including vegetation and impervious surface lead to the underestimation of ET due to the low resolution of vegetation data. ET estimates may involve large errors for mixed pixels with different land use types, especially for the QRB with highly fragmented land due to rapid urbanization (Fig S5); and iii) simplification and assumption in product parameterization schemes may also lead to errors. For example, one single parameter value for temperature and vapor pressure deficit was used globally in MOD16 to determine stomata closure for grassland. Such treatments may not be appropriate for modeling ET in humid areas (He and Shao 2014; Jiang et al. 2017; Wu G. et al. 2013). In summary, these deficiencies suggest that MOD16 ET products are not suitable for assessing the actual ET in highly urbanized watersheds. Although the SSEBop ET results compared reasonably well with the raw MODIS ET product (i.e., MOD16A2) (Fig S5), its low resolution still limits its application in small-scale (such as watershed scale) urbanization analysis.

Compared with MOD16 ET and SSEBop, our ET estimates using the SEBAL model covers all areas with or without vegetation and thus are more accurate at a watershed level. In addition, our ET estimates also have a higher resolution (250 m by this study *vs* 1000 m by MOD16 ET and SSEBop), which better represents the ET characteristics with different land covers. We argue that, compared with global large-scale ET products, energy balance models might be most reliable in estimating ET in urban areas when properly parameterized. Our study suggests that only comprehensive use of high-precision ground observation data, land use data and meteorological data can accurately estimate ET in urban areas. However, the eddy flux network and ET measurements for unban conditions are sparse and we have limited knowledge of energy balance in urban areas (Lipson, et al., 2022).

Uncertainties of the SEBAL model

The main uncertainty of SEBAL model comes from remote sensing input data and the accuracy of retrieved land surface variables (Li et al. 2009). The remote sensing imageries are instantaneous one-shot of the Earth surface and were mostly useful during clear-sky days. The potential issues related to the 8-day MODIS products provided by NASA LP-DACC and their influences on the accuracy of simulations should not be ignored in spite large progress has been made in improving remote sensing products (Li et al. 2009).

Another uncertainty in SEBAL model is the empirical formulations for estimating soil heat flux (*G)* using a fixed coefficient (i.e., a proportion of net radiation). The uncertainty may be particularly large when calculating *G* over water bodies and built-up land. Future work should focus on improving the land surface parameters required by SEBAL model. The present study explored new multiple criteria to select hot and cold pixels that are critical for estimating *H* (Long et al. 2011) by integrating land surface temperature, land use characteristics, and NDVI. However, when determining extreme pixels, the errors may still exist and may affect the model accuracy.

To our knowledge, this study represents the first time that SEBAL model was applied in a river basin that have experienced long-term rapid urbanization and climate change in the humid southern China. Future field studies need to further validate the energy balances for all land uses (e.g., flux measurements across urbanization gradient) and improve the representations of ecohydrological processes (e.g., surface and subsurface energy and water transport).

Conclusions

This research quantified spatial patterns of ET and other energy fluxes in a rapidly urbanized watershed with complex land uses. We parameterized the energy balance model SEBAL to explicitly explore the long-term (19 years) dynamic connections between land use change and energy and water balance change at the watershed level. This remote sensing-based modeling study found that the Qinhuai River Basin in southern China experienced rapid land use change in urban–rural interface (URI) area, resulting in a significant reduction in evapotranspiration but an increase in sensible heat and soil heat fluxes during the growing season from 2001 to 2019. The change in energy partitioning at the watershed scale was dominated by URI area. Our study suggests that URI area is the 'hot spots' of ecohydrological change within a heterogeneous basin. The rapid change in energy and water balance in URI area is likely to bring a series of chain reactions in environmental changes, such as the increase in storm runoff, non-point source water pollution, and UHI and UDI as identified in our previous studies in this basin.

The new process-based understanding reported in this study helps properly parameterize regional climate and ecohydrological models to guide urban planning. Effective watershed management should target urban–rural interface areas to mitigate the negative impacts of urbanization on both air and water. These management measures may include minimizing vegetation removal, enhancing urban forestry, wetland conservation and restoration, and other 'Nature-based Solutions' that maximize ET, atmospheric cooling, and urban runoff retention.

Acknowledgements We acknowledge China Meteorological Data Service Center (http://data.cma.cn/en) for providing weather observation data, Ministry of Natural Resources of the People's Republic of China for Chinese map (http://bzdt.ch.mnr.gov.cn/index.html), USGS Earth Explorer site (https://earthexplorer.usgs.gov/) for Landsat imageries and Land Processes Distributed Active Archive Center (https://lpdaac.usgs.gov/data_access/data_pool) for MODIS product datasets, and USGS FEWS NET SSEBop Actual Evapotranspiration Products (Version 5.0) (https://earlywarning.usgs.gov/fews/product/458).

Author contributions GS and LH conceived the ideas, led manuscript conceptualization and designed the methodology. KJ and MQ led data collection, analysis, and interpretation. RT and XH assisted with data collection and created figures. The first draft of the manuscript was written by KJ, MQ and all authors commented on previous versions of the manuscript. All authors gave final approval for publication.

Funding LH is funded by the National Natural Science Foundation of China (grants 42061144004, 41977409, and 41877151) and National Key Research and Development Program of China (grant 2019YFC1510202). GS is supported by the Southern Research Station, United States Department of Agriculture Forest Service.

Data availability The data generated and analysed during the current study are available from the corresponding author on reasonable request.

Declarations

Conflict of interest The authors have no relevant financial or non-financial interests to disclose.

References

Allen RG, Pereira LS, Raes D, Smith M (1998) Crop evapotranspiration - Guidelines for computing crop water requirements - FAO Irrigation and drainage paper 56.

Bastiaanssen WGM, Menenti M, Feddes RA, Holtslag AAM (1998a) A remote sensing surface energy balance algorithm for land (SEBAL). 1 formulation. J Hydrol 212–213:198–212

Bastiaanssen WGM, Pelgrum H, Wang J, Ma Y, Morenoc JF, Roerink GJ, van der Wal T (1998b) A remote sensing surface energy balance algorithm for land (SEBAL). 2 validation. J Hydrol 212–213:213–229

Bastiaanssen WGM, Ahmad M, Chemin Y (2002) Satellite surveillance of evaporative depletion across the Indus Basin. Water Resour Res 38:1273

Bastiaanssen WGM, Noordman EJM, Pelgrum H, Davids G, Thoreson BP, Allen RG (2005) SEBAL model with remotely sensed data to improve water-resources management under actual field conditions. J Irrig Drain Eng 131:85–93

Browder JO (2002) The urban-rural interface: urbanization and tropical forest cover change. Urban Ecosyst 6:21–41

Chang Y, Ding Y, Zhao Q, Zhang S (2017) Remote estimation of terrestrial evapotranspiration by Landsat 5 TM and the SEBAL model in cold and high-altitude regions: a case study of the upper reach of the Shule River Basin, China. Hydrol Process 31:514–524

Chen H, Zhang Y, Yu M, Hua W, Sun S, Li X, Gao C (2015) Large-scale urbanization effects on eastern Asian summer monsoon circulation and climate. Clim Dyn 47:117–136

Crago RD (1996) Conservation and variability of the evaporative fraction during the daytime. J Hydrol 180:173–194

DeWalle DR, Swistock BR, Johnson TE, McGuire KJ (2000) Potential effects of climate change and urbanization on mean annual streamflow in the United States. Water Resour Res 36:2655–2664

Du J, Song K, Wang Z, Zhang B, Liu D (2013) Evapotranspiration estimation based on MODIS products and surface energy balance algorithms for land (SEBAL) model in Sanjiang Plain, Northeast China. Chin Geogra Sci 23:73–91

Ebel BA, Mirus BB (2014) Disturbance hydrology: challenges and opportunities. Hydrol Process 28:5140–5148

Fang S, Gertner GZ, Sun Z, Anderson AA (2005) The impact of interactions in spatial simulation of the dynamics of urban sprawl. Landsc Urban Plan 73:294–306

Fang D, Hao L, Cao Z, Huang X, Qin M, Hu J, Liu Y, Sun G (2020) Combined effects of urbanization and climate change on watershed evapotranspiration at multiple spatial scales. J Hydrol. https://doi.org/10.1016/j.jhydrol.2020.124869

Feng X, Sun G, Fu B, Su C, Liu Y, Lamparski H (2012) Regional effects of vegetation restoration on water yield across the Loess Plateau, China. Hydrol Earth Syst Sci 16:2617–2628

Fratini G, Mauder M (2014) Towards a consistent eddy-covariance processing: an intercomparison of EddyPro and TK3. Atmos Meas Tech 7:2273–2281

Gao G, Chen D, Xu C, Simelton E (2007) Trend of estimated actual evapotranspiration over China during 1960–2002. J Geophys Res. https://doi.org/10.1029/2006JD008010

Gao G, Xu C, Chen D, Singh VP (2012) Spatial and temporal characteristics of actual evapotranspiration over Haihe River basin in China. Stoch Env Res Risk Assess 26:655–669

Gao Z, He J, Dong K, Li X (2017) Trends in reference evapotranspiration and their causative factors in the West Liao River basin, China. Agric for Meteorol 232:106–117

Gu C, Hu L, Zhang X, Wang X, Guo J (2011) Climate change and urbanization in the Yangtze River Delta. Habitat Int 35:544–552

Guan Y, Zheng F, Zhang P, Qin C (2014) Spatial and temporal changes of meteorological disasters in China during 1950–2013. Nat Hazards 75:2607–2623

Hao L, Sun G, Liu Y, Wan J, Qin M, Qian H, Liu C, Zheng J, John R, Fan P, Chen J (2015) Urbanization dramatically altered the water balances of a paddy field-dominated basin in southern China. Hydrol Earth Syst Sci 19:3319–3331

Hao L, Huang X, Qin M, Liu Y, Li W, Sun G (2018) Ecohydrological processes explain Urban Dry Island effects in a Wet Region, Southern China. Water Resour Res 54:6757–6771

Hara Y, Takeuchi K, Okubo S (2005) Urbanization linked with past agricultural landuse patterns in the urban fringe of a deltaic Asian mega-city: a case study in Bangkok. Landsc Urban Plan 73:16–28

He T, Shao Q (2014) Spatial-temporal variation of terrestrial evapotranspiration in China from 2001 to 2010 Using MOD16 products. J Geo-Inf Sci. https://doi.org/10.3724/SP.J.1047.2014.00979

Hsieh D, Xia Y, Wray L, Qian D, Pal A, Dil JH, Osterwalder J, Meier F, Bihlmayer G, Kane CL, Hor YS, Cava RJ, Hasan MZ (2009) Observation of unconventional quantum spin textures in topological insulators. Science 323:919–922

Huang J, Li Y, Fu C, Chen F, Fu Q, Dai A, Shinoda M, Ma Z, Guo W, Li Z, Zhang L, Liu Y, Yu H, He Y, Xie Y, Guan X, Ji M, Lin L, Wang S, Yan H, Wang G (2017) Dryland climate change: recent progress and challenges. Rev Geophys 55:719–778

Huang X, Hao L, Sun G, Yang Z, Li W, Chen D (2022) Urbanization aggravates effects of global warming on local atmospheric drying. Geophys Res Lett. https://doi.org/10.1029/2021GL095709

Jackson RB, Jobbágy EG, Nosetto MD (2009) Ecohydrology in a human-dominated landscape. Ecohydrology 2:383–389.

Jackson RD, Idso SB, Reginato RJ, Pinter PJ (1981) Canopy temperature as a crop water stress indicator. Water Resour Res 17:1133–1138

Jackson RD, Hatfield JL, Reginato RJ, Idso SB, Pinter PJ (1983) Estimation of daily evapotranspiration from one time-of-day measurements. Agric Water Manag 7:351–362.

Jiang Y, Wang W, Zhou Z (2017) Evaluation of MODIS MOD16 evaportranspiration product in Chinese River Basins. J Nat Resour 32:517–528.

Kiptala JK, Mohamed Y, Mul ML, Van der Zaag P (2013) Mapping evapotranspiration trends using MODIS and SEBAL model in a data scarce and heterogeneous landscape in Eastern Africa. WATER RESOURCES RESEARCH 49:8495–8510.

Krzywinski M, Schein J, Birol I, Connors J, Gascoyne R, Horsman D, Jones SJ, Marra MA (2009) Circos: an information aesthetic for comparative genomics. Genome Res 19:1639–1645.

Lee Y, Kim S (2016) The modified SEBAL for mapping daily spatial evapotranspiration of South Korea using three flux towers and terra MODIS data. Remote Sens. https://doi.org/10.3390/rs8120983

Li B, Chen Y, Li W, Cao Z (2011) Remote sensing and the SEBAL model for estimating evapotranspiration in the Tarim River. Acta Geogr Sin 66:1230–1238

Li C, Sun G, Caldwell PV, Cohen E, Fang Y, Zhang Y, Oudin L, Sanchez GM, Meentemeyer RK (2020a) Impacts of Urbanization on watershed water balances across the conterminous United States. Water Resour Res 56:1–19.

Li C, Sun G, Cohen E, Zhang Y, Xiao J, McNulty SG, Meentemeyer RK (2020b) Modeling the impacts of urbanization on watershed-scale gross primary productivity and tradeoffs with water yield across the conterminous United States. J Hydrol. https://doi.org/10.1016/j.jhydrol.2020.124581

Li G, Zhang F, Jing Y, Liu Y, Sun G (2017) Response of evapotranspiration to changes in land use and land cover and climate in China during 2001–2013. Sci Total Environ 596–597:256–265.

Li M, Ma Z (2014) Sensible and iatent heat flux variability and response to dry-wet soil moisture zones across China. Boundary-Layer Meteorol 154:157–170.

Li S, Zhao W (2010) Satellite-based actual evapotranspiration estimation in the middle reach of the Heihe River Basin using the SEBAL method. Hydrol Process 24:3337–3344.

Li Z, Liu X, Ma T, Kejia D, Zhou Q, Yao B, Niu T (2013) Retrieval of the surface evapotranspiration patterns in the alpine grassland-wetland ecosystem applying SEBAL model in the source region of the Yellow River. China Ecol Model 270(64):75

Li ZL, Tang R, Wan Z, Bi Y, Zhou C, Tang B, Yan G, Zhang X (2009) A review of current methodologies for regional evapotranspiration estimation from remotely sensed data. Sensors (basel) 9:3801–3853.

Lipson M, Grimmond S, Best M, Chow W, Christen A, Chrysoulakis N, Coutts A, Crawford B, Earl S, Evans J, Fortuniak K, Heusinkveld BG, Hong J-W, Hong J, Järvi L, Jo S, Kim Y-H, Kotthaus S, Lee K, Masson V, McFadden JP, Michels O, Pawlak W, Roth M, Sugawara H, Tapper N, Velasco E, Ward HC (2022) Harmonized gap-filled datasets from 20 urban flux tower sites. Earth Syst. Sci. Data 14(11):5157–78

Liu B, Xu M, Henderson M, Gong W (2004) A spatial analysis of pan evaporation trends in China, 1955–2000. J Geophys Res. https://doi.org/10.1029/2004JD004511

Liu B, Chen X, Zhang L, Liu D (2007) Optimal deployment of water resources for seasonal water shortage area in South China. J Hydraul Eng 38:732–737.

Liu X, Yang S, Xu J, Zhang J, Liu J (2017) Effects of soil heat storage and phase shift correction on energy balance closure of paddy fields. Atmósfera 30:39–52.

Long D, Singh VP, Li Z (2011) How sensitive is SEBAL to changes in input variables, domain size and satellite sensor? J Geophys Res. https://doi.org/10.1029/2011JD016542

Mazrooei A, Reitz M, Wang D, Sankarasubramanian A (2021) Urbanization impacts on evapotranspiration across various spatio-temporal scales. Earth's Future 9:e2021EF002045.

Mkhwanazi M, Chávez J, Andales A, DeJonge K (2015) SEBAL-A: a remote sensing ET algorithm that accounts for advection with limited data. Part II: test for transferability. Remote Sensing 7:15068–15081.

Mu Q, Zhao M, Running SW (2011) Improvements to a MODIS global terrestrial evapotranspiration algorithm. Remote Sens Environ 115:1781–1800.

Qin M, Hao L, Sun L, Liu Y, Sun G (2019) Climatic controls on watershed reference evapotranspiration varied during 1961–2012 in Southern China. J Am Water Resour Assoc 55:189–208.

Senay GB, Bohms S, Singh RK, Gowda PH, Velpuri NM, Alemu H, Verdin JP (2013) Operational evapotranspiration mapping using remote sensing and weather datasets: a new parameterization for the SSEB approach. J Am Water Resour Assoc 49:577–591.

Singh RK, Irmak A, Irmak S, Martin DL (2008) Application of SEBAL model for mapping evapotranspiration and estimating surface energy fluxes in South-Central Nebraska. J Irrig Drain Eng 134:273–285.

Sun G, Lockaby GB (2012) Water Quantity and Quality at the Urban-Rural Interface. Urban-Rural Interfaces, pp 29–48. https://doi.org/10.2136/2012.urban-rural.c3

Sun G, McNulty SG, Lu J, Amatya DM, Liang Y, Kolka RK (2005) Regional annual water yield from forest lands and its response to potential deforestation across the southeastern United States. J Hydrol 308:258–268.

Sun G, Alstad K, Chen J, Chen S, Ford CR, Lin G, Liu C, Lu N, McNulty SG, Miao H, Noormets A, Vose JM, Wilske B, Zeppel M, Zhang Y, Zhang Z (2011a) A general predictive model for estimating monthly ecosystem evapotranspiration. Ecohydrology 4:245–255.

Sun Z, Wei B, Su W, Shen W, Wang C, You D, Liu Z (2011b) Evapotranspiration estimation based on the SEBAL model in the Nansi Lake Wetland of China. Math Comput Model 54:1086–1092.

Tang RL et al (2013) Spatial-scale effect on the SEBAL model for evapotranspiration estimation using remote sensing data. Agri For Meteorol 174:28–42

Tse JWP, Yeung PS, Fung JCH, Ren C, Wang R, Wong MMF, Cai M (2018) Investigation of the meteorological effects of urbanization in recent decades: a case study of major cities in Pearl River Delta. Urban Climate 26:174–187.

Vejre H, Jensen FS, Thorsen BJ (2010) Demonstrating the importance of intangible ecosystem services from peri-urban landscapes. Ecol Complex 7:338–348.

Verma SB, Baldocchi DD, Anderson DE, Matt DR, Clement RJ (1986) EDDY FLUXES OF CO2 WATER VAPOR, AND SENSIBLE HEAT OVER A DECIDUOUS FOREST. Bound-Layer Meteorol 36:71–91.

Vose JM, Sun G, Ford CR, Bredemeier M, Otsuki K, Wei X, Zhang Z, Zhang L (2011) Forest ecohydrological research in the 21st century: what are the critical needs? Ecohydrology 4:146–158.

Wang J, Yang S, He T, Lu H (2004) Technological methods of information interpretation and analysis of land use change in urban fringe area—taking Wuxi City as an example. Prog Geogr 23:1–9

Wang L, Liu J, Sun G, Wei X, Liu S, Dong Q (2012a) Water, climate, and vegetation: ecohydrology in a changing world. Hydrol Earth Syst Sci 16:4633–4636.

Wang X, Zhang C, Wei J (2012b) Application of the SEBAL method in water resources management in the Yellow River Delta of China. Desalin Water Treat 19:212–218.

Wang X, Yang M, Wan G (2013) Temporal-Spatial distribution and evolution of surface sensible heat flux over Qinghai-Xizang Plateau during Last 60 years. Plateau Meteorol 32:1557–1567.

Wu D, Zhan S, Tu M, Zheng J, Li Y, Guo Y, Peng H (2016) New trends and practical research on the sponge cities with Chinese characteristics. China Soft Sci 1:79–97

Wu G, Liu Y, Zhao X, Ye C (2013) Spatio-temporal variations of evapotranspiration in Poyang Lake Basin using MOD16 products. Geogr Res 32:617–627

Wu J (2013) Landscape sustainability science: ecosystem services and human well-being in changing landscapes. Landscape Ecol 28:999–1023.

Wu J, Hobbs R (2002) Key issues and research priorities in landscape ecology: an idiosyncratic synthesis. Landscape Ecol 17:355–365.

Xiang K, Lia Y, Horton R, Feng H (2020) Similarity and difference of potential evapotranspiration and reference crop evapotranspiration – a review. Agric Water Manag 232:106043

Xu C, Gong L, Jiang T, Chen D, Singh VP (2006) Analysis of spatial distribution and temporal trend of reference evapotranspiration and pan evaporation in Changjiang (Yangtze River) catchment. J Hydrol 327:81–93.

Xu L, Shi Z, Wang Y, Zhang S, Chu X, Yu P, Xiong W, Zuo H, Wang Y (2015) Spatiotemporal variation and driving forces of reference evapotranspiration in Jing River Basin, northwest China. Hydrol Process 29:4846–4862.

Yan Z, Zhou D (2023) Rural agriculture largely reduces the urban heating effects in China: a tale of the three most developed urban agglomerations. Agric for Meteorol 331:109343

Yang J, Mei X, Huo Z, Yan C, Ju H, Zhao F, Liu Q (2015) Water consumption in summer maize and winter wheat cropping system based on SEBAL model in Huang-Huai-Hai Plain, China. J Integr Agric 14:2065–2076.

Yang L, Feng Q, Yin Z, Wen X, Si J, Li C, Deo RC (2016) Identifying separate impacts of climate and land use/cover change on hydrological processes in upper stream of Heihe River, Northwest China. Hydrol Process 31:1100–1112.

Yang Y, Shang S, Jiang L (2012) Remote sensing temporal and spatial patterns of evapotranspiration and the responses to water management in a large irrigation district of North China. Agric for Meteorol 164:112–122.

Yang Y, Anderson MC, Gao F, Hain CR, Semmens KA, Kustas WP, Noormets A, Wynne RH, Thomas VA, Sun G (2017) Daily landsat-scale evapotranspiration estimation over a forested landscape in North Carolina, USA, using multi-satellite data fusion. Hydrol Earth Syst Sci 21:1017–1037.

Yang Y, Anderson M, Gao F, Hain CR, Noormets A, Sun G, Wynne R, Thomas V, Sun L (2020) Investigating impacts of drought and disturbance on evapotranspiration over a forested landscape in North Carolina, USA using high spatiotemporal resolution remotely sensed data. Remote Sensing of Environment. https://doi.org/10.1016/j.rse.2018.12.017

Zhan C, Xia J, Li Z, Niu C (2005) Modelling the spatial distribution of actual terrestrial evapotranspiration using a hydrological and meteorological approach. Regional Hydrological Impacts of Climatic Change—Hydroclimatic Variability. IAHS Publication, Wallingford, p 296

Zhang J, Zhang Y, Sun G, Song C, Li J, Hao L, Liu N (2022) Climate variability masked greening effects on water yield in the yangtze river basin during 2001–2018. Water Resour Res 58:e2021WR030382.

Zhang L, Yao Y, Wang Z, Jia K, Zhang X, Zhang Y, Wang X, Xu J, Chen X (2017b) Satellite-derived spatiotemporal variations in evapotranspiration over Northeast China during 1982–2010. Remote Sens 9:1140.

Zhang T, Chen Y (2017a) Analysis of dynamic spatiotemporal changes in actual evapotranspiration and its associated factors in the Pearl River Basin based on MOD16. Water. https://doi.org/10.3390/w9110832

Zhang YL, Qin BQ, Chen WM (2004) Analysis of 40 year records of solar radiation data in Shanghai, Nanjing and Hangzhou in Eastern China. Theoret Appl Climatol 78:217–227.

Zhang J, Zhang Y, Sun G, Song C, Dannenberg MP, Li J, Liu N, Zhang K, Zhang Q (2021) Vegetation greening significantly reduced the capacity of water supply to China's South-North water diversion project. Hydrol Earth Syst Sci 25:5623–5640.

Zheng Q, Hao L, Huang X, Sun L, Sun G (2020) Effects of urbanization on watershed evapotranspiration and its components in Southern China. Water. https://doi.org/10.3390/w12030645

Zhou D, Zhao S, Liu S, Zhang L (2014) Spatiotemporal trends of terrestrial vegetation activity along the urban development intensity gradient in China's 32 major cities. Sci Total Environ 488–489:136–145.

Zhou D, Zhao S, Zhang L, Liu S (2016a) Remotely sensed assessment of urbanization effects on vegetation phenology in China's 32 major cities. Remote Sens Environ 176:272–281.

Zhou D, Li D, Sun G, Zhang L, Liu Y, Hao L (2016b) Contrasting effects of urbanization and agriculture on surface temperature in Eastern China. J Geophys Res: Atmos 121:9597–9606.